MODAL ANALYSIS OF COMPLEX TURBULENT FLOW

Octavian Frederich
Department of Computational Fluid Dynamics and Aeroacoustics
Berlin University of Technology
Müller-Breslau-Str. 12, 10623 Berlin
octavian.frederich@tu-berlin.de

Dirk M. Luchtenburg
Department of Mechanical and Aerospace Engineering
Princeton University
Princeton, NJ 08544
dluchten@princeton.edu

ABSTRACT

Three-dimensional turbulent flow is highly complex and few investigations have focused on the use of modal decompositions to characterise important physical phenomena and interactions. In this paper, we consider the Proper Orthogonal Decomposition (POD) and Dynamic Mode Decomposition (DMD). We show how the correlation matrix which is needed for POD can be re-used in the computation of the DMD modes. After two introductory examples, we focus on modal decompositions of a complex turbulent flow around a wall-mounted finite cylinder at $Re = 2 \cdot 10^5$. Finally, the usefulness of both decompositions is discussed.

INTRODUCTION AND OBJECTIVES

The analysis of the dynamics in turbulent flow is still a major challenge due to the unsteady, three-dimensional and stochastic nature of turbulence. It is important to characterise and quantify the properties of turbulence, so that desired and undesired effects such as strong mixing or high drag, can be identified, understood and possibly controlled. A method based analysis is indispensable because of the complex spatial and temporal interaction in turbulent flow. Here, modal decompositions are used to analyse the data, which can subsequently be used for the development of low-dimensional models which capture the essential flow physics.

Two different types of modal analysis are considered, namely the Proper Orthogonal Decomposition (POD) and the Dynamic Mode Decomposition (DMD). We show how the correlation matrix which is needed for POD can be re-used in the computation of the DMD modes. Both methods are applied to the turbulent flow field around a finite circular cylinder mounted on a ground plate. The results of the conceptually different approaches (POD and DMD) are compared in order to examine their strengths and weaknesses.

MODAL DECOMPOSITION

The main goal in this paper is the extraction of (large-scale) coherent motion from a given data set. To this end modal decomposition techniques are used to analyse the spatial structure and temporal evolution separately. Starting point is a set of N flow fields obtained by experiment or simulation. For simplicity, consider the fluctuating part (around the mean) of an equidistantly (with timestep Δt) sampled velocity vector field $\mathbf{u}(\mathbf{x},t)$. The N snapshots $\mathbf{u}_j = \mathbf{u}(\mathbf{x}_i,t_j)$ are assembled columnwise in a $P \times N$ data matrix

$$\mathbf{U} = \left[\, \mathbf{u}_1 \, \dots \, \mathbf{u}_{N-1} \; \mathbf{u}_N \,\right], \tag{1}$$

where P is the number of grid points times the number of considered variables n. Alternatively, the following equivalent notation can be used $\{\mathbf{u}(\mathbf{x}_i,t_j)\}$ where $i = 1,\dots,P/n$ and $j = 1,\dots,N$.

The data ensemble can be represented as a superposition of M modes or motion patterns

$$\mathbf{u}(\mathbf{x}_i,t_j) = \sum_{m=1}^{M} \mathbf{b}_m(\mathbf{x}_i)\, a_m(t_j) \qquad \text{or} \qquad \mathbf{U} = \mathbf{X}\mathbf{T}, \tag{2}$$

where $\mathbf{T}$ contains the temporal amplitudes $a_m(t_j)$, $\mathbf{X}$ the spatial modes $\mathbf{b}_m(\mathbf{x}_i)$ and $M \ll N$, since only modes describing large scale coherent motion are retained. Mathematically, a variety of basis functions can be chosen for either the temporal amplitudes or the spatial modes, e.g. Fourier functions, polynomials, etc. In this paper the basis functions are physically motivated and data driven. Two methods are used: the Proper Orthogonal Decomposition and the Dynamic Mode Decomposition. The POD method was used to identify so-called coherent structures (modes) in turbulent flows by Berkooz et al. (1993). POD can be considered a purely statistical method where the modes are obtained from maximisation of the energy over the complete data ensemble. In the DMD method the snapshots are assumed to be generated by a linear dynamical system, which implies that the extracted basis is characterised by growth rate and frequency content of the snapshots. Both methods are detailed in the literature, e.g. POD by Berkooz et al. (1993) and DMD by Rowley et al. (2009); Schmid (2010). Here we show the partial congruence of POD and DMD and how the (weighted) POD correlation matrix can be used in the DMD computation.

Proper Orthogonal Decomposition (POD)

Premise for the POD is spatial or temporal correlation (coherence) of the flow field. Since POD is a statistical method which maximises the variance over all snapshots, it is ideally performed using the fluctuating flow field values, i.e. the time-averaged flow field is subtracted.

The first step in the POD method is the computation of a (weighted) correlation matrix

$$\mathbf{C} = \mathbf{U}^T \mathbf{W} \mathbf{U}, \tag{3}$$

where $\mathbf{W}$ is a weighting matrix. In our case, this is a diagonal matrix where the weights are given by the local cell volumes corresponding to each grid point, i.e. $\mathbf{W} = \operatorname{diag}\left[V_1 \ \dots \ V_P \right]$. The entries of $C_{ij} = (\mathbf{u}_i, \mathbf{u}_j) = \mathbf{u}_i^T \mathbf{W} \mathbf{u}_j$ describe the (global) covariance of two snapshots at different moments in time.

The second step is to find the eigenvalues and eigenvectors of $\mathbf{C}$

$$\mathbf{C}\,\mathbf{v}_i = \lambda_i \mathbf{v}_i, \quad i = 1, \dots, N. \tag{4}$$

Since $\mathbf{C}$ is symmetric, positive-semidefinite, all the eigenvalues λ_i are real and nonnegative, i.e. $\lambda_1 \geq \lambda_2 \geq \dots \geq \lambda_N \geq 0$, and the eigenvectors $\mathbf{v}_i$ are orthogonal. The eigenvalues are proportional to the fluctuation energy associated with each amplitude / mode in the modal decomposition.

The temporal amplitudes are scaled versions of the normalised (orthonormal) eigenvectors $\mathbf{v}_i$

$$\mathbf{T} = \begin{bmatrix} a_1(t_j) \\ \vdots \\ a_N(t_j) \end{bmatrix} = \begin{bmatrix} \mathbf{v}_1^T \sqrt{\lambda_1} \\ \vdots \\ \mathbf{v}_N^T \sqrt{\lambda_N} \end{bmatrix}. \tag{5}$$

The POD modes can now be computed by inversion of (2)

$$\mathbf{X} = \mathbf{U}\mathbf{T}^{-1} = \mathbf{U} \begin{bmatrix} \dfrac{\mathbf{v}_1}{\sqrt{\lambda_1}} & \cdots & \dfrac{\mathbf{v}_N}{\sqrt{\lambda_N}} \end{bmatrix}. \tag{6}$$

These modes are orthonormal with respect to the weighted inner product, i.e. $\mathbf{X}^T \mathbf{W} \mathbf{X} = \mathbf{I}$.

Since the POD extracts a bi-orthogonal basis which is sorted with respect to the variance or energy contained, it is not always straightforward to interpret the physical meaning of the amplitudes and modes in the decomposition. In complex flows, different temporal and spatial scales are often present in one amplitude / mode. Thus, POD allows for frequency and scale mixing, but also for variable frequency content.

Dynamic Mode Decomposition (DMD)

The goal of the DMD method is the extraction of dynamic information, e.g. temporal evolution of spatial structures, from a given snapshot sequence. It is assumed that the snapshots are generated by a linear discrete-time model

$$\mathbf{u}_{k+1} = \mathrm{e}^{\tilde{\mathbf{A}}\Delta t} \mathbf{u}_k = \mathbf{A}\mathbf{u}_k. \tag{7}$$

It is also assumed that the snapshots become linearly dependent for an increasing number of snapshots, such that the last snapshot $\mathbf{u}_N$ can be constructed (or approximated) by a linear combination of all previous snapshots, i.e.

$$\mathbf{u}_N = \sum_{j=1}^{N-1} c_j \, \mathbf{u}_j. \tag{8}$$

Summarising, we have

$$\left[\mathbf{u}_2 \ \dots \ \mathbf{u}_N \right] = \mathbf{A} \left[\mathbf{u}_1 \ \dots \ \mathbf{u}_{N-1} \right] = \tilde{\mathbf{U}}\tilde{\mathbf{C}}, \tag{9}$$

with the the companion matrix $\tilde{\mathbf{C}} = \begin{bmatrix} 0 & 0 & \cdots & 0 & c_1 \\ 1 & 0 & & 0 & c_2 \\ 0 & 1 & & 0 & c_3 \\ \vdots & & \ddots & & \vdots \\ 0 & \cdots & 0 & 1 & c_{N-1} \end{bmatrix}$ and the reduced data matrix $\tilde{\mathbf{U}} = \left[\mathbf{u}_1 \ \dots \ \mathbf{u}_{N-1} \right]$. The weights c_i are computed such that the error is minimised (least-square problem).

For the DMD method, we also need to solve an eigenproblem

$$\tilde{\mathbf{C}}\,\tilde{\mathbf{v}}_i = \tilde{\lambda}_i \tilde{\mathbf{v}}_i, \quad i = 1, \dots, N-1. \tag{10}$$

The eigenvalues $\tilde{\lambda}_i$ are a subset of the eigenvalues of $\mathbf{A}$ and the corresponding eigenvectors can be constructed by

$$\mathbf{b}_i = \left[\mathbf{u}_1 \ \dots \ \mathbf{u}_{N-1} \right] \tilde{\mathbf{v}}_i. \tag{11}$$

In general, the eigenvalues $\tilde{\lambda}_i$ and the eigenvectors $\mathbf{b}_i$ are complex numbers. The eigenvectors of $\mathbf{A}$ are called DMD modes and are assembled in a matrix

$$\tilde{\mathbf{X}} = \tilde{\mathbf{U}}\tilde{\mathbf{V}} = [\mathbf{b}_1 \dots \mathbf{b}_{N-1}]. \tag{12}$$

The DMD amplitudes can be computed by inversion of the eigenvector matrix $\tilde{\mathbf{V}}$ (compare (2) with (12)) or by spanning the first snapshot in the basis of the DMD modes, i.e. $\mathbf{u}_1 = \sum_{i=1}^{N-1} d_i \mathbf{b}_i$, which leads to a Vandermonde matrix (see Rowley et al., 2009). Let the temporal amplitudes be given by

$$\tilde{\mathbf{T}} = \begin{bmatrix} \tilde{a}_1(t_j) \\ \vdots \\ \tilde{a}_N(t_j) \end{bmatrix}. \tag{13}$$

In the continuous domain, the frequency f_i and growth rate σ_i of a DMD mode $\mathbf{b}_i$ are obtained by

$$f_i = \Im\left[\ln(\lambda_m)\right] / \Delta t / 2\pi \tag{14}$$

$$\sigma_i = \Re\left[\ln(\lambda_m)\right] / \Delta t. \tag{15}$$

In general, the dynamic modes are non-orthogonal. They can be sorted by frequency, mode norm or growth rate. DMD provides one frequency and growth rate per mode. An unconverged time-averaged flow field is indicated by a non-constant temporal amplitude corresponding to $f_i = 0$.

Combining POD and DMD

As a first step in the analysis of turbulence, a POD of the snapshot ensemble is computed. A low-dimensional model of the snapshot ensemble can be build from the results (examples in Luchtenburg, 2010) and the correlation matrix can be used in the calculation of DMD as shown in the following.

The construction of the correlation matrix (3) is expensive because of the huge amount of data. It is therefore convenient to use (partial) results of this decomposition step for further analysis. For DMD, we need to construct a companion matrix with weights c_i given by (8). Taking the inner product with snapshot $\mathbf{u}_i$ on both sides of (8), we have

$$(\mathbf{u}_i, \mathbf{u}_N) = \sum_{j=1}^{N-1} (\mathbf{u}_i, \mathbf{u}_j)\, c_j, \quad i = 1, \ldots, N-1. \tag{16}$$

If we choose the same inner product as used for computation of the correlation matrix in (3), then (16) simplifies to

$$C_{iN} = \sum_{j=1}^{N-1} C_{ij}\, c_j, \quad i = 1, \ldots, N-1. \tag{17}$$

Note that the weights c_i can now be calculated by a weighted least-square problem $(\tilde{\mathbf{U}}^T \mathbf{W} \tilde{\mathbf{U}})\, \mathbf{c} = \tilde{\mathbf{U}}^T \mathbf{W} \mathbf{u}_N$, where the matrix and right-hand-side easily follow from the POD correlation matrix.

RESULTS

Firstly the capabilities of POD and DMD are demonstrated using two simple generic examples and secondly results for the complex turbulent flow around a wall-mounted cylinder are presented. For the cylinder flow two different cases are considered: (i) POD and DMD of the velocity field in a subdomain at the cylinder top on a coarse grid and (ii) POD and DMD of the pressure field (based on the POD correlation matrix) of the complete domain with the original highly-resolved grid and wake dynamics.

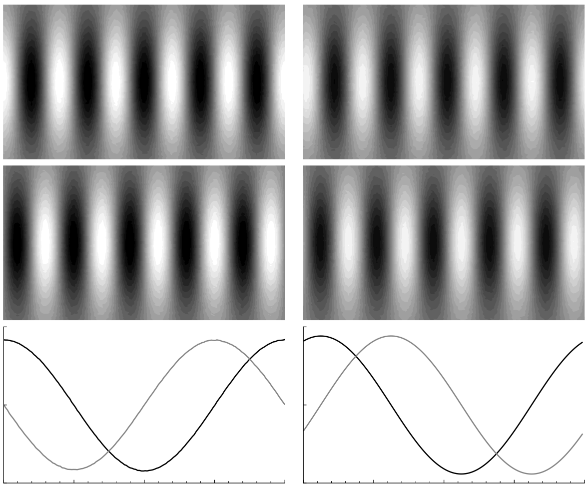

(a) POD (b) DMD

Figure 1. Dominant modes and their temporal amplitudes for a single travelling wave.

POD and DMD of simple examples

As a first simple example, a harmonic travelling wave is considered. The snapshots are given by $u_1(x_i, y_i, t_j) = \mathrm{e}^{-(y_i/b)^2} \cos(kx_i - \omega t_j)$ for a single period $T = 2\pi/\omega$. The parameters are chosen as $b = 0.02$, $k = \pi/b$ and $\omega = 20\pi$. The time period is equidistantly sampled by 150 time steps and the spatial resolution is 100×100 cells in a domain of $10b \times 2.5b$. To test the robustness of the methods, the snapshots are contaminated by strong white noise with a variance of 40% with respect to the snapshot mean.

The spatial structure and temporal amplitudes of the dominant mode pairs obtained by POD and DMD are shown in figure 1. Both techniques extract the correct spatial pattern and the sinusoidal temporal behaviour. (The only difference is a nonrelevant phase shift.) DMD provides a frequency of $f = 10.0023$ and a growth rate $\sigma = -0.0019$ for this example. The exact result of 10 is obtained for zero noise.

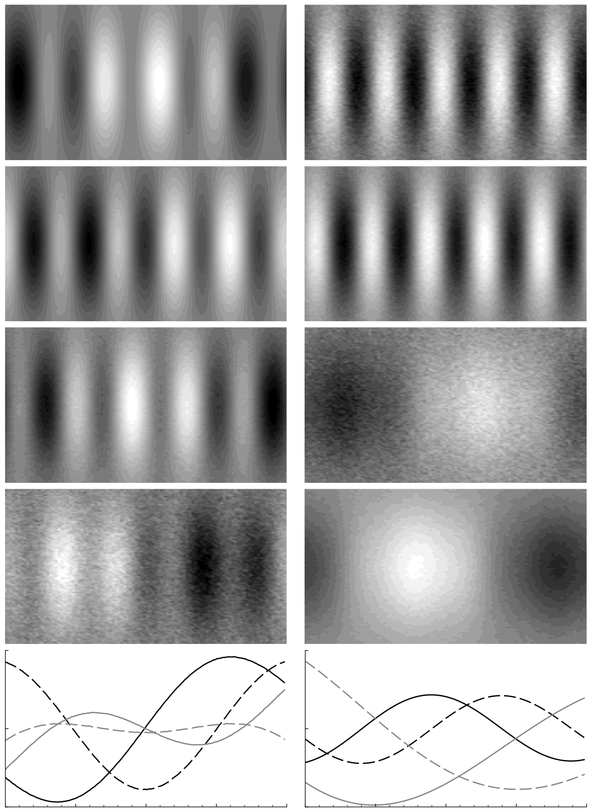

(a) POD (b) DMD

Figure 2. Dominant modes and their temporal amplitudes for two superimposed travelling waves.

Another simple example, comprising two superimposed waves is given by $u_2(x_i, y_i, t_j) = u_1(x_i, y_i, t_j) + 1.1 \left[\mathrm{e}^{-(y_i/b)^2} \cos(\frac{kx_i}{5} - \frac{\omega t_j}{2}) \right]$ with the same parameters as before. Since the simulation time is also unchanged, only half a time period of the lower frequency is resolved. The dominant POD and DMD modes are presented in figure 2. The DMD method does not filter out all noise, but the frequencies are well separated and the harmonics are almost perfectly recovered. The strong noise particularly contaminates the real part of the underresolved long-wave harmonic. The extracted frequencies are 10.0591 and 4.9132 with small negative growth rates. The clarity of the structures and convergence of the frequencies improve significantly with reduced noise level.

The POD results show relatively strong scale and frequency mixing for this relatively simple example. The second mode pair does not correctly represent the structure of the second harmonic. The temporal amplitudes are partially not even sinusoidally. Also the spatial structure of the first dominant mode pair does only partially represent the travelling wave pattern. Note that POD is not designed for optimality with respect to scale and frequency separation but for most energetic global structures. In this particular case, the approach suffers from underresolved temporal dynamics, which implies inaccurate statistics. Thus the results for POD can be improved with an extended time interval.

POD and DMD of complex turbulent flow

The results presented below are obtained from the numerically predicted flow around a wall-mounted finite cylinder, which has been analysed extensively by Frederich (2010). The flow field with a Reynolds number of $2 \cdot 10^5$ (based on the diameter of the cylinder) has been simulated employing a large-eddy simulation (LES). For the current section a database of 700 snapshots of an isolated region at the top of the cylinder is used. The time step is $\Delta t = 0.1D/U_\infty$, and the velocity fields have been resampled to an equidistant Cartesian grid of 390 000 cells in order to reduce numerical effort and to replace the original highly-resolved and curvilinear grid.

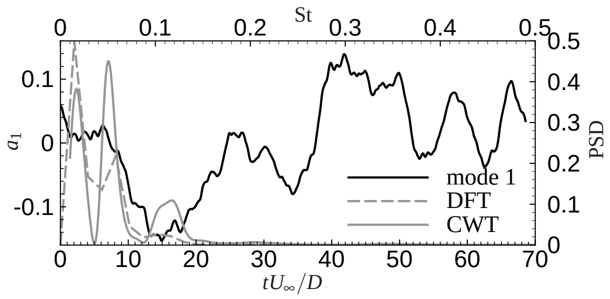

(a) time coefficient and frequency spectrum

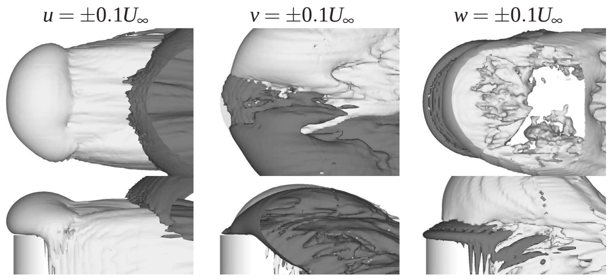

(b) mode 1

Figure 3. Dominant POD mode 1 at the cylinder top (spatial structure shown by isosurfaces of the velocity components)

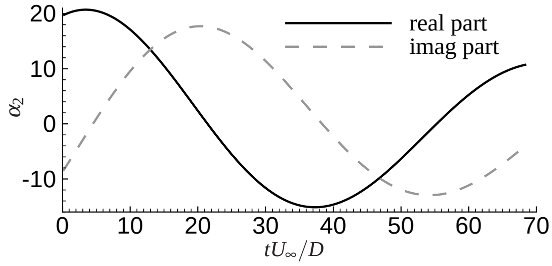

(a) time coefficient

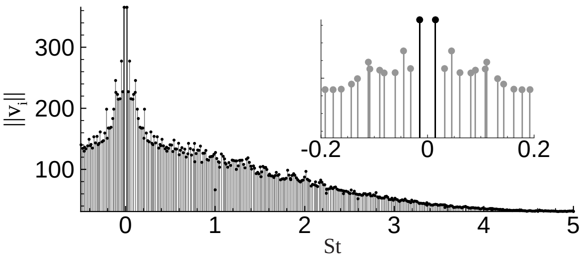

(b) DMD frequency spectrum

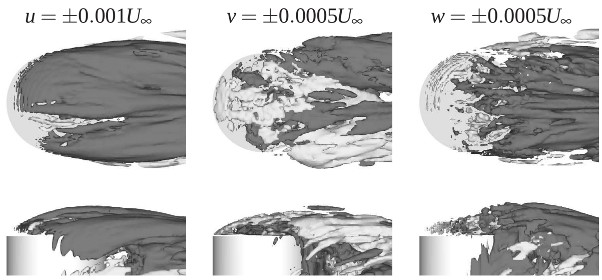

(c) real part of mode 2

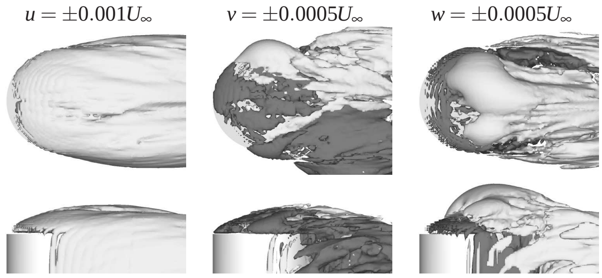

(d) imaginary part of mode 2

Figure 4. Dominant DMD mode 2 at the cylinder top (spatial structure shown by isosurfaces of the velocity components)

The fluctuations and vortical motion in the top region of the cylinder represent only a small amount of fluctuation energy compared to the wake structures. Thus, a POD of the (complete) global flow field could not sufficiently dissect local phenomena and restriction to a subdomain of interest is mandatory. Due to the stochastic nature of the flow on the cylinder top and the (time-averaged) global correlation, POD is not able to (clearly) separate fluid motion with respect to frequency or wavelength. The dominant, most energetic mode, shown in figure 3, is isolated as single mode with spectral components at Strouhal numbers of $\mathrm{St} = 0.015$ and 0.055. The first frequency is associated with the vertical flapping motion of the separated shear layer and the second one has been identified as an intermodulation artefact of dominant wake patterns (details in Frederich, 2010). Nearly all higher modes do not admit physical interpretation due to a high level of frequency (and scale) mixing which spans over the whole spectrum of St $= 0...1.5$. For the current configuration, POD has shown to be inapt for the decomposition of the highly complex turbulent region on the cylinder top into (distinct) individual coherent structures; only dominant global patterns can be identified but without clear differentiation.

A DMD of the flow near the cylinder top results in an almost non-changing (converged) mean flow and dominant low-frequency harmonics at St $= 0.015$ and 0.045 with small damping rates. As illustrated in figure 4 for the predominant harmonic, the DMD method yields unmixed frequencies. On the one hand this avoids scale mixing as is the case for POD, but on the other hand small frequency variations can result in several similar modes in narrow frequency bands (like FFT). The spatial structure of the mode itself is comparable to the POD mode, especially for the imaginary part (compare figures 3 b and 4 c,d). The harmonic describes changes in size and topology of the recirculation region on the cylinder top, which are associated with the flapping state of the adjacent shear layer (and a fixed frequency). The most interesting observation is that the entire phenomenon has been solely captured by this mode, as the DMD spectrum does not include further modes of this frequency component (insert in figure 4 b).

POD and POD-based DMD of complex turbulent flow

Results shown in this section are computed for the original LES simulation grid of $12.3 \cdot 10^6$ cells and 2 744 snapshots of the flow around the wall-mounted finite cylinder. For such a large snapshot ensemble $\mathbf{U}$, the computation of the DMD requires parallelisation or smart utilisation of algebraic features which to reduce computational load. Thus, in contrast to the previous section, we now use the POD correlation matrix for calculation of the weights c_i in the companion matrix (see (17)). This allows for a relatively cheap computation of the DMD. Previous investigations revealed that the influence of volume weighting, implied by the weighting matrix $\mathbf{W}$, has a small impact in general. In particular, the sensitivity increases for wall-bounded coherence resolved by near-wall refinement of typical numerical grids. A remaining problem is the a-priori mode sortation. Sortation based on the mode norm is not convenient since all modes need to be computed which is not feasible because of the very large dimensions.

For the current case we compute (a subset of) the eigenvalues of $\mathbf{A}$ and only compute the DMD modes in a particular frequency band. A natural parallelisation for the computation of the modes is given by the block-structured domain, where the same weights to construct the DMD modes are provided for each block. Here, for simplicity the results of the scalar pressure field are shown.

The wake of the flow around the wall-mounted cylinder is dominated by a strongly deformed vortex street which is associated with a frequency of St ≈ 0.165 (for details see Frederich et al., 2011). This pattern is mostly contained in the dominant POD mode pair, but mixed with other large coherent large structures. In particular the temporal amplitudes reveal the involvement of spectral components at St ≈ 0.2. The comparison of the dominant POD mode and associated DMD mode (with $St = 0.165$) in figure 5 demonstrates that the modes are very similar. Nevertheless the DMD approach en-

$p = \pm 0.10\rho U_\infty^2$

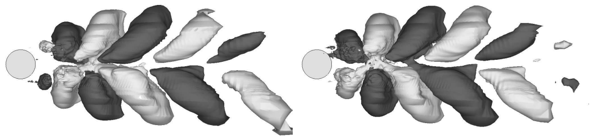

(a) dominant POD mode pair

$p = \pm 0.25\rho U_\infty^2$

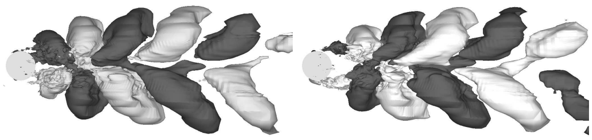

(b) dominant DMD mode

Figure 5. Dominant POD and DMD modes within the full spatial domain around the finite cylinder

ables extraction of frequency-specific phenomena. The DMD modes (with vortices in dark) associated with St ≈ 0.2 are presented in figure 6. These structures, reveal another variant of sideways vortex shedding which cannot directly be obtained by POD. Note that harmonic filtering of POD modes succeeds only partially, because the frequencies of interest are of similar magnitude and can hardly be separated by the required bandpass filter. On the other hand the DMD approach cannot account directly for slight variations of the harmonics. This results in a variety of related modes in narrow spectral bands.

$p = \pm 0.25\rho U_\infty^2$

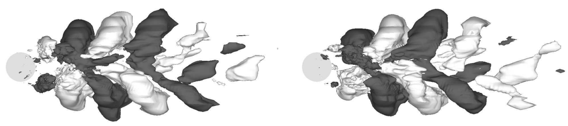

Figure 6. DMD mode corresponding to frequency St ≈ 0.2 for the flow around the finite cylinder

In general the DMD method yields a variety of harmonic modes with corresponding amplitudes which are characterised by a single (fixed) frequency and a growth rate. The (varying) mean flow is obtained as a single (real) mode times a modal (temporal) amplitude, whereas in the POD method the ensemble mean is directly computed from the snapshots. As already mentioned, employing DMD transient data, e.g. a change of the mean flow, is indicated by a non-constant modal amplitude (nonzero growth rate).

DISCUSSION AND OUTLOOK

The focus of this contribution is the modal decomposition of turbulent flow fields employing POD and DMD. Application of both methods has become increasingly popular for the analysis of complex turbulent flow and shear flow phenomena over the last years. Strengths and weaknesses of POD and DMD as well as the similarity between them are discussed in order to transfer knowledge gained from application to a complex turbulent flow field.

Sample results have been shown to highlight some inherent properties of POD and DMD. The POD extracts coherence based on correlation of the snapshots and is best performed in a relatively large domain (see Frederich, 2010). It does not clearly separate frequencies and scales, but effectively filters out coherent structures based on kinetic energy content and provides temporal amplitudes which are directly related to particular flow dynamics. The DMD method yields pure harmonic phenomena, with distinct frequencies and growth rates, but cannot describe temporal varying frequencies. Both methods capture dominant phenomena (characterised by large energy content). In addition, DMD provides stability properties.

We suggest that first a POD of the data is performed, which can be used for further postprocessing like filtering, modelling and phase-averaging. A subsequent DMD is relatively cheap because the POD correlation matrix can be used for construction of the companion matrix and then the (weighted) least-squares problem does not require the use of the high-dimensional data matrix.

Our motivation for this work is a framework for modal post-processing. Therefore we will continue to analyse data with diverse parameters (e.g. volume weighting, DMD mode order, etc.) in order to establish guidelines for the modal analysis of complex turbulent flows.

REFERENCES

Berkooz, G., Holmes, P. and Lumley, J. L., 1993, ”The proper orthogonal decomposition in the analysis of turbulent flows”, Annual Review of Fluid Mechanics, vol. 25, pp. 539–575.

Frederich, O., 2010, ”Numerische Simulation und Analyse turbulenter Strömungen am Beispiel der Umströmung eines Zylinderstumpfes mit Endscheibe”, PhD thesis, ISTA, TU Berlin.

Frederich, O., Scouten, J., Luchtenburg, D.M., Thiele, F., 2011, ”Large-scale dynamics in the flow around a finite cylinder with ground plate”, Fluid Dynamics Research, vol. 43, 015504.

Luchtenburg, D.M., 2010, ”Low-dimensional modelling and control of separated shear flows”, PhD thesis, ISTA, TU Berlin.

Rowley, C. W., Mezić, I., Bagheri, S., Schlatter, P. & Henningson, D. S., 2009, ”Spectral analysis of nonlinear flows”, Journal of Fluid Mechanics, vol. 641, pp. 115–127.

Schmid, P. J., 2010, ”Dynamic mode decomposition of numerical and experimental data”, Journal of Fluid Mechanics, vol. 656, pp. 5–28.